



PERGAMON

Aerosol Science 33 (2002) 943–959

Journal of
Aerosol Science

www.elsevier.com/locate/jaerosci

Numerical modeling of silicon oxide particle formation and transport in a one-dimensional low-pressure chemical vapor deposition reactor

S.-M. Suh^a, M.R. Zachariah^{a,b}, S.L. Girshick^{a,*}

^a*Department of Mechanical Engineering, University of Minnesota, Minneapolis, MN 55455, USA*

^b*Department of Chemistry, University of Minnesota, Minneapolis, MN 55455, USA*

Received 17 August 2001; accepted 14 January 2002

Abstract

A numerical model is presented for particle formation and transport during low-pressure chemical vapor deposition of silicon dioxide films from silane and oxygen. A detailed chemical kinetics approach was used to model silicon oxide clustering that leads to homogeneous nucleation. A moment-type aerosol dynamics model was developed, which includes particle growth by surface reactions and coagulation, and particle transport by convection, diffusion and thermophoresis, assuming a lognormal particle size distribution function. A chemical clustering mechanism was coupled to the aerosol dynamics model in an axisymmetric stagnation–flow reactor. Simulations were conducted to predict steady-state spatial distributions of major particle characteristics such as particle concentration, diameter and volume fraction. The effects of various system parameters were assessed for conditions around 1.5 Torr (200 Pa), 800°C, 200 sccm and an inlet oxygen-to-silane ratio of 20. Model predictions are shown to be in good agreement with experimental data and indicate that, unlike the case of particle formation in silane pyrolysis, the results are relatively insensitive to temperature. On the other hand, we observe a large sensitivity to pressure change, which is corroborated by experiment. © 2002 Elsevier Science Ltd. All rights reserved.

Keywords: Homogeneous nucleation; Chemical nucleation; Silane oxidation; Semiconductor processing; Chemical vapor deposition

1. Introduction

Chemical vapor deposition (CVD) of SiO₂ films from silane and oxygen is widely used in the integrated circuit fabrication industry. Although many CVD processes are operated at low pressures

* Corresponding author. Tel.: +1-612-625-5315; fax: +1-612-625-4344.

E-mail address: slg@tc.umn.edu (S.L. Girshick).

(~ 1 Torr (133 Pa)), there is experimental evidence (Liehr & Cohen, 1992) that even at low pressures particle contamination from gas-phase nucleation can be a significant problem. This problem will become more severe as the so-called “critical size of killer particles” decreases along with the characteristic feature size, which is projected to be about 50 nm by 2003 (Semiconductor Industry Association, 1999). It thus becomes increasingly important to increase our understanding of the kinetics of particle formation, growth and transport. Moreover, the development of experimentally verified numerical models will provide a valuable tool for cost-effective process screening and optimization.

There is a well-established body of research in the field of homogeneous nucleation of particles in a complex chemical system, namely soot formation and the subsequent oxidation in hydrocarbon flames. One of the most sophisticated mechanisms was developed by Frenklach and coworkers (Frenklach & Warnatz, 1987) in this C–H–O chemistry. They proposed a hydrogen-abstraction-carbon-addition mechanism for the growth of gas-phase hydrocarbon species. Soot particles formed by this mechanism then experience surface chemistry, coagulation, diffusion, convection and external body forces according to the combustion conditions involved. The aerosol dynamics was addressed by a moment-type model. In contrast, Smooke, McEnally, Pfefferle, Hall, and Colket (1999) employed a simplified approach with regard to the kinetics of soot nucleation, based on an empirical estimate of the formation rate of two- and three-ringed aromatic species. However, they considered a higher level of complexity in fluid mechanics by formulating a two-dimensional, axisymmetric, laminar, coflow diffusion flame. To model soot dynamics, they adopted a sectional approach where the number of sections varied according to soot size/density parameters.

Less work has been reported from a detailed chemical kinetics standpoint for silicon-based systems. Swihart and Girshick (1999) presented a detailed kinetics mechanism for gas-phase nucleation of hydrogenated silicon particles during silane pyrolysis, which was subsequently coupled to an aerosol dynamics model to investigate silicon hydride particle formation over a wide range of operating conditions (Girshick, Swihart, Suh, Mahajan, & Nijhawan, 2000). Suh, Zachariah, and Girshick (2001) developed a clustering mechanism for silicon oxide particle formation in the more complex Si–H–O chemistry, and predicted the time-dependent behavior of particle characteristics in a zero-dimensional batch reactor. Although the computationally inexpensive zero-dimensional model allowed for the efficient development of the mechanism and provided insights into the pathways for growth, it did not address the importance of transport processes. In this study we extend the previous work by Suh et al. (2001), and investigate the silicon oxide particle formation process with a steady-state one-dimensional reactor model.

In the following section, we present descriptions of the kinetics mechanism of silicon oxide clustering, the reactor model, and the aerosol dynamics model. Steady-state simulation results and comparisons with experimental data are presented in Section 3.

2. Model description

2.1. Clustering mechanism

A detailed description of our reaction mechanism is provided in our previous work (Suh et al., 2001). Briefly, the base silane oxidation mechanism is taken from the work of Babushok, Tsang, Burgess, and Zachariah (1998), which was developed to model self-ignition and flame propagation

during silane combustion at atmospheric pressure. We applied quantum Rice–Ramsperger–Kassel (QRRK) theory (Dean, 1985) to this base mechanism to estimate the pressure dependence of the unimolecular reactions whose activation energies are known. A number of additional reaction pathways for intermediate $\text{Si}_x\text{H}_y\text{O}_z$ species (Zachariah & Tsang, 1995) were included to complete our base silane oxidation mechanism for the pressure range of interest (~ 1 Torr).

Based on the detailed silane oxidation chemistry, nucleation kinetics were modeled by a chemical clustering approach where silicon oxides are allowed to cluster to form larger species by sequential polymerization steps. Given the complexity inherent in this three-element (Si–H–O) system, our approach is to assume that the species most likely to contribute the dominant fraction of the nucleating mass are those silicon-containing species that are produced in the highest concentrations. For our system, SiO, SiO₂, SiH₂O and HSiOOH were identified as the four most abundant species from our preliminary kinetics calculations. These species were treated as monomers for subsequent clustering processes. Firstly, the following two classes of reversible self-clustering reactions of SiO and SiO₂ were considered, as expressed in Eqs. (1) and (2):



for $1 \leq n \leq 9$, $1 \leq m \leq 9$, and $n + m \leq 10$.

We also included the contributions of SiH₂O and HSiOOH and of their dimers through the two classes of irreversible dehydrogenation reactions given in Eqs. (3) and (4). SiH₂O and HSiOOH and their dimers were assumed to insert without an energy barrier into SiO and SiO₂ clusters, respectively, based on the similarities of the ground-state molecular structures of the monomer and the dimer, and comparing SiH₂O to SiO and HSiOOH to SiO₂ (Zachariah & Tsang, 1995).



for $1 \leq n \leq 9$, $m = 1$ or 2 , and $n + m \leq 10$.

Clusters containing more than 10 silicon atoms, i.e., for the case when $n + m > 10$ in reactions (1)–(4), were assumed to form irreversibly via the same set of clustering reactions, and the particle nucleation rate was set equal to the sum of their production rates. Once formed, these smallest size “particles” are no longer considered gas molecules. They are treated as having the properties of bulk material, and their growth and transport are solved in an aerosol dynamics model, presented below.

The choice of size 10 at which to truncate the chemical clustering mechanism is arbitrary. At the temperatures of interest SiO and SiO₂ have such low vapor pressures that the monomers are already above the “critical nucleus size”. However, if one treats the monomer already as a “particle” (as often found in the literature in such cases) then a great deal of chemical information is lost, for example the contributions to clustering of reactions (3) and (4), which we find to be important. The clustering mechanism inherently contains more detailed chemical information than the aerosol dynamics model. Therefore, the larger the size that is included in the clustering mechanism, the more accurate, in principle, will be the results. Treating clusters containing as few as 11 silicon atoms as “particles” possessing properties of the bulk material is obviously an approximation (although, as discussed in Suh et al. (2001), the enthalpies of formation per molecule of (SiO)₁₀ and (SiO₂)₁₀

are predicted to be remarkably close to their bulk values). However, the computational expense increases dramatically as the truncation point is increased. Furthermore, the level of uncertainty in the kinetic mechanism does not warrant increasing the truncation point to too high a size. Size 10 was chosen as a reasonable compromise among these competing factors. The quantitative results are somewhat affected by the choice of truncation size, because cluster growth is treated differently in the aerosol dynamics model (as chemical vapor deposition of a silicon oxide film) than in the chemical clustering mechanism (where clusters are treated the same as molecules). Thus, for example, if the chemical clustering mechanism were extended from size 10 to size 20, the results would be somewhat different, especially regarding growth from size 10 to size 20.

The pressure-dependent rate constants for the four classes of clustering reactions in Eqs. (1)–(4) were obtained by utilizing generic radical recombination rate constants (Dean, 1985) and QRRK theory (Dean, 1985; Westmoreland, Howard, Longwell, & Dean, 1986). As the clustering reactions were assumed to be barrierless, we assumed the activation energies of the dissociation reactions of (1) and (2) to be temperature-independent and equal to the corresponding heats of reaction at 1073 K. We treated the activation energy for a given reaction as a constant, as the heat of reaction is only a weak function of temperature, and consistent with the level of uncertainty inherent in this approach to barrierless reactions.

Cluster enthalpies and entropies are required to calculate equilibrium constants that are needed to obtain the reverse rate constants of reactions (1) and (2). Ab initio calculations for smaller SiO and SiO₂ clusters, up to the hexamer and tetramer, respectively, are available from the literature (Zachariah & Tsang, 1995; Nayak, Rao, Khanna, & Jena, 1998). Standard statistical mechanics methods (McQuarrie, 1976) were used to compute enthalpies and entropies based on these data sets for ground-state clusters. The properties of larger clusters, containing up to ten silicon atoms, were estimated by extrapolating a linear least-squares fit on the smaller oxide clusters.

Our model for single particle growth assumes that molecules and radicals arriving at a surface from the gas phase are influenced only by the local chemical environment, and thus cannot distinguish between the surface of a silicon oxide “particle” and that of a growing silicon oxide “film”. Thus, we modeled particle growth by utilizing available information on chemical vapor deposition of silicon oxide films. We took a simple approach to model the surface reactions in this study. The reactivity of each gas species at the surface was represented by assigning a sticking probability that is multiplied by the thermal collision frequency to yield a rate constant. The values of species sticking probabilities were estimated based on the work of Meeks, Larson, Ho, Apblett, Han, Edelberg, & Aydil, (1998) and Buss, Ho, and Weber (1993). Among the major silicon-containing gas species in our mechanism, SiO₂ was assigned a sticking probability of unity, while SiH₂O and HSiOOH and their dimers were assumed to be nonreactive on surfaces. A unity sticking probability was also assigned to all the other radical species as well as to the clusters of SiO and SiO₂. The SiO molecule requires special attention. Buss et al. (1993) used molecular beams and laser-induced fluorescence to measure the reactivity of SiO on a depositing silicon oxide film, and found it to be near zero, but suggested a conservative upper bound of 0.25. To mimic “a value near zero” we assigned a value of 10⁻⁴. The sensitivity of the final results to uncertainties in the SiO sticking probability is discussed in Section 3 below.

As CVD of silicon oxide films with the stoichiometry of SiO_x ($x = 1-2$) was assumed, the growth rate at either a particle surface or the film surface (on top of the deposition substrate) was obtained from the sum of the surface production rates of SiO and SiO₂ and their clusters, as given

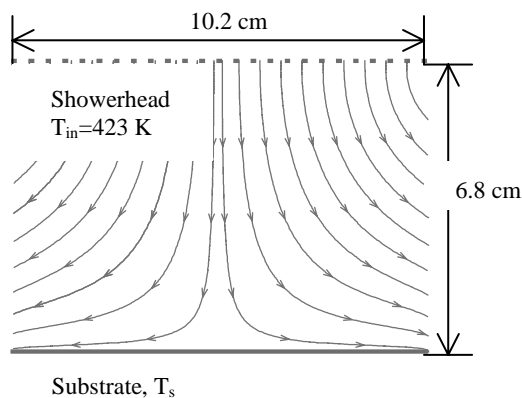


Fig. 1. A schematic representation of the computational geometry for an axisymmetric stagnation-point flow between two parallel plates.

in Eq. (5).

$$G = \sum_k \frac{\dot{s}_k W_k}{\rho_b}, \quad k = (\text{SiO})_n \text{ or } (\text{SiO}_2)_n, \quad 1 \leq n \leq 10, \quad (5)$$

where \dot{s}_k , W_k and ρ_b are, respectively, net surface production rate, molecular weight of the k th species, and mass density of bulk material. ρ_b was assumed to be 2.33 g cm^{-3} . We employed the formalism in the CHEMKIN software (Kee, Rupley, Meeks, & Miller, 1996) to implement the homogeneous and heterogeneous chemical kinetics.

2.2. Reactor model

The Gaseous Electronics Conference (GEC) reference cell (Hargis Jr. et al., 1994) was modeled by approximating the flow in the center region of the reactor to be an axisymmetric stagnation-point flow between two parallel plates. Fig. 1 shows a schematic of the computational geometry for the flow. A detailed derivation of the governing equations in this geometry can be found in Coltrin, Kee, and Evans (1989). The governing equations are reduced to one-dimensional form through a similarity transformation (Schlichting, 1979). Gas reactants are introduced at a given mass flow rate through the inlet showerhead, which is separated from the bottom substrate by a distance of 6.8 cm. The substrate is usually maintained at an elevated temperature ($\sim 800^\circ\text{C}$), which provides the necessary energy input for chemical reactions to occur in the gas phase and at the surface.

From a rigorous point of view, the presence of particles in the gas phase should invoke a two-phase flow formulation. However, because the particle loadings are extremely low, we can assume that particles do not affect the flow characteristics. Furthermore the small size of the particles being considered here (low Stokes number) implies that the particles behave the same as molecules with respect to convection.

We modified SPIN (Coltrin, Kee, Evans, Meeks, Rupley, & Grcar, 1991), the CHEMKIN application program for one-dimensional stagnation-point flow CVD reactors, which solves for the flow and temperature fields in this geometry. One of the major modifications required was to the species

mass conservation equation, as expressed in Eq. (6), so as to consider species depletion from the gas phase due to nucleation and particle surface reactions:

$$\rho \frac{\partial Y_k}{\partial t} + \rho u \frac{\partial Y_k}{\partial z} = -\frac{\partial}{\partial z} (\rho Y_k V_k) + \left(\dot{\omega}_k^g + \dot{\omega}_k^n + \frac{A}{V} \dot{s}_k \right) W_k, \quad k = 1, 2, \dots, K_g, \quad (6)$$

where ρ , u , Y_k , and V_k are, respectively, the mass-averaged mixture density, mixture axial velocity, mass fraction and diffusion velocity of the k th species. In the second term on the right-hand side, $\dot{\omega}_k^g$, $\dot{\omega}_k^n$ and \dot{s}_k are the net production rates of the k th species due to gas-phase chemical reactions, homogeneous nucleation, and heterogeneous reactions on particle surfaces, respectively. K_g is the total number of gas species. A is the total particle surface area and V is the total volume of the gas. Eq. (6) together with the standard mixture mass, momentum, and energy conservation equations constitute the governing equations for the flow, temperature and gas mass continuity. To self-consistently determine the surface-to-volume ratio, A/V , in Eq. (6) one needs to solve the aerosol general dynamic equation (GDE) (Friedlander, 2000) together with the other governing equations.

2.3. A moment-type aerosol dynamics model

To obtain features of the particle size distribution, one needs to solve the aerosol GDE. A moment method is adopted in this study for its computational efficiency. In the moment method one solves for only the first few moments of the particle size distribution function, which we assumed to follow the general form of a unimodal lognormal function throughout the process. It should be noted that this is an approximation, as if nucleation is not fast enough, or if nucleation occurs in several different places, then multi-modal particle size distributions can result, in which case the assumption of a unimodal lognormal model would tend to underpredict the mean particle size. The first few moments of a lognormal particle size distribution are directly related to the quantities that are usually of most interest, including the total particle concentration, the mean particle size, and the width of the size distribution. The k th moment of the particle size distribution is defined by $M_k = \int_0^\infty v_p^k n(v_p, t) dv_p$, where v_p is particle volume and $n(v_p, t)$ is the particle size distribution function. Following the approach of Lee, Chen, and Gieseke (1984) and Pratsinis and Kim (1989), the time evolution of the k th moment can be obtained by integrating the aerosol GDE multiplied by particle volume over the size range. The result can be written as

$$\begin{aligned} \frac{\partial M_k}{\partial t} + \nabla \cdot (\vec{u} M_k) = & [\dot{M}_k]_{\text{diffusion}} + [\dot{M}_k]_{\text{thermophoresis}} + [\dot{M}_k]_{\text{coagulation}} \\ & + [\dot{M}_k]_{\text{surface growth}} + [\dot{M}_k]_{\text{nucleation}}. \end{aligned} \quad (7)$$

The contributing processes of convection, diffusion, thermophoresis, coagulation, surface growth and nucleation are included in Eq. (7). Because the substrate is typically heated with respect to the inlet showerhead, a temperature gradient exists along the axial flow direction. This requires inclusion of a term (the second term on the right-hand side (RHS)) to account for thermophoretic transport of particles. The fourth term on the RHS represents single-particle growth due to chemical reactions of gas molecules at the particle surface. The last term accounts for the generation of the smallest

particles—“nuclei”—through homogeneous nucleation, whose rate is taken equal to the production rate of silicon oxide clusters containing more than ten silicon atoms, as discussed in the section on the chemical clustering model. For the pressure regime of interest, particles are much smaller than the mean free path for collisions in the gas. Thus, free-molecule-regime expressions were used for the surface growth and coagulation terms.

We present here expressions for the two transport terms on the RHS of Eq. (7), diffusion and thermophoresis. The diffusion term in Eq. (7) can be written as

$$\begin{aligned} [\dot{M}_k]_{\text{diffusion}} &= \int_0^\infty v_p^k \nabla \cdot [D \nabla n(v_p, t)] dv_p \\ &= \nabla \cdot (K \nabla M_{k-2/3}), \end{aligned} \quad (8)$$

where $K = D \cdot v_p^{2/3}$ and

$$D = \frac{(3/4\pi)^{1/3} k_B T}{v_p^{2/3} \rho \sum_{k=1}^{K_g} Y_k \bar{c}_k (1 + \pi \alpha_k / 8)}$$

where D is the particle diffusivity in the free-molecule regime multi-component expression (Waldmann & Schmidt, 1966), k_B is the Boltzmann constant, and c_k and α_k are the mean thermal speed and the accommodation coefficient of the k th gas species, respectively. Generally, $\alpha_k = 0.9$ in the free-molecule regime (Friedlander, 2000).

The thermophoresis term can be expressed as

$$\begin{aligned} [\dot{M}_k]_{\text{thermophoresis}} &= \int_0^\infty v_p^k \nabla \cdot [\mathbf{V}_{\text{th}} n(v_p, t)] dv_p \\ &= \nabla \cdot (\mathbf{V}_{\text{th}} M_k). \end{aligned} \quad (9)$$

The thermophoretic velocity, \mathbf{V}_{th} , can be written as $\mathbf{V}_{\text{th}} = -0.554(\mu/\rho T) \nabla T$ (Friedlander, 2000), where μ is gas viscosity. Solutions for the first three moments in Eq. (7), i.e., $k = 0-2$, provide the particle number concentration, M_0 , particle volume fraction, M_1 , and the geometric standard deviation of the particle size distribution,

$$\sigma_g = \exp\left(\frac{1}{3} \ln^{1/2}\left(\frac{M_0 M_2}{M_1^2}\right)\right).$$

Expressions for the other terms in Eq. (7) can be found in Suh et al. (2001).

2.4. Solution procedure

The set of governing equations accounting for the flow, temperature, species mass conservation and aerosol dynamics must be solved simultaneously because of the cross-coupling terms. For solutions to the steady axisymmetric stagnation–point flow, the transient terms in Eqs. (6) and (7) were removed, and TWOPNT (Grcar, 1996), a boundary-value-problem solver based on the modified Newton method, was used to search iteratively for converged solutions. A typical run took several CPU hours on an SGI Origin 2000 supercomputer.

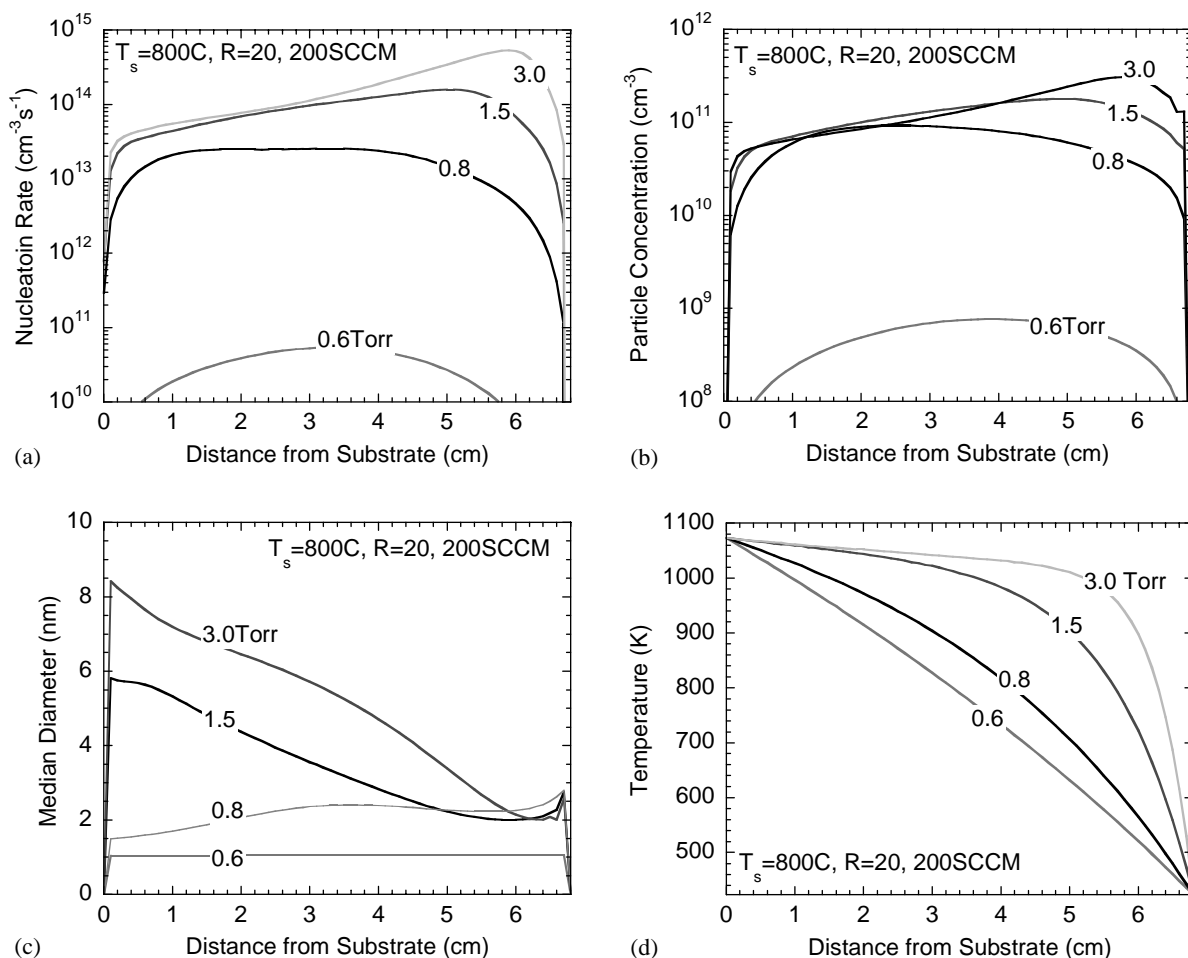


Fig. 2. Pressure effect on particle nucleation rate, concentration and size at substrate temperature of $T_s = 800^\circ\text{C}$, oxygen-to-silane ratio of $R = 20$ and an inlet flow rate of 200 sccm: (a) axial distributions of particle nucleation rate, (b) axial distributions of particle concentration, (c) axial distributions of particle median diameter and (d) axial distributions of temperature.

3. Results and discussion

Fig. 2 shows the predicted distributions of particle concentration and diameter along the axial direction for various settings of the total pressure. The substrate temperature (T_s) is set to 800°C with an inlet 200 sccm flow of an oxygen–silane mixture at 20-to-1 ratio (R). Fig. 2(a) and (b) shows the predicted distributions of particle nucleation rate and concentration, respectively, while varying the total pressure from 0.6 to 3 Torr (80–400 Pa). A dramatic increase of particle production is predicted for a small pressure change from 0.6 to 0.8 Torr (80–107 Pa), and then particle production becomes less sensitive to the pressure change at higher pressures. It should be noted that the pressure change in this figure is accompanied by changes in the partial pressures of the reactants (SiH_4 and

O₂) and in the residence time of the flow, as R and the flow rate have been kept constant for the calculation. Compared to the nucleation rate curves in Fig. 2(a), Fig. 2(b) shows that coagulation narrows the variation in particle concentration with regard to the pressure change. As constrained by the boundary conditions, the particle concentration is calculated to be zero at both the inlet and the substrate, and the location of the peaks corresponds to the location where particle nucleation is most active. For the range of conditions considered in Fig. 2, “nucleation” occurs primarily through the following three routes: $\text{Si}_9\text{O}_{18} + (\text{HSiOOH})_2 \rightarrow \text{particle}$, $\text{Si}_9\text{O}_9 + (\text{SiH}_2\text{O})_2 \rightarrow \text{particle}$, and $\text{Si}_{10}\text{O}_{10} + \text{SiO} \rightarrow \text{particle}$.

In Fig. 2(c) we show that the median particle diameter is predicted to be < 10 nm for the entire range of pressures considered. At 0.6 Torr, the median particle size is predicted to remain very close to the size of 11-silicon-atom “particles”, as coagulation and surface growth at this pressure are negligible. At 0.8 Torr the particle size is predicted to peak at an axial position close to the showerhead, whereas at 1.5 and 3.0 Torr the particle size peaks right at the substrate. This difference is caused mainly by the effect of pressure on the temperature profile, as shown in Fig. 2(d), and in turn on the thermophoretic force. At 0.8 Torr there is a strong temperature gradient that pushes particles away from the substrate, and a strong convective force pushing particles toward the substrate. These two forces are balanced close to the showerhead, so that particles located in this region experience close-to-zero net velocity, allowing them time to grow. At higher pressures the temperature gradient near the substrate is significantly reduced by exothermic chemistry, as shown in Fig. 2(d), so that the thermophoretic force becomes negligible relative to the convective force. In this case particles continue to grow as they are transported toward the substrate.

The extreme pressure sensitivity at the low-pressure end shown in Fig. 2 was not found in our previous zero-dimensional modeling of this system (Suh et al., 2001). We attribute it to the combined synergistic effects of several factors associated with the pressure change, including Brownian diffusion of key radical species, which is absent from the zero-dimensional model and which is strongly pressure dependent. The silane oxidation chemistry is initiated at the showerhead by direct barrierless insertion of oxygen into the silyl radical, SiH_3 , which is produced by the interaction of SiH_4 with radical species. The resulting $(\text{SiH}_3)\text{-(O}_2)$ complex undergoes a number of unimolecular chain-branching reactions to produce highly reactive radicals, which in turn play a key role in the destruction of silane. H and OH are the key radicals that control the silane decomposition process. The rate of silane decomposition has a direct influence on the production of the two primary growth species, $(\text{HSiOOH})_2$ and $(\text{SiH}_2\text{O})_2$, which then affect the clustering process sequentially through reactions (3) and (4).

Fig. 3 shows the calculated distributions of H concentrations as total pressure is varied with various combinations of system parameters associated with the pressure change: flow residence time and the inlet partial pressures of silane and oxygen. Comparing Fig. 3(a)–(c), one sees that the H concentration is strongly affected by both residence time and the inlet reactant partial pressures, especially in the pressure range from 0.6 to 0.8 Torr, and that the effect of varying the reactant partial pressures is greater than that of varying the residence time.

Fig. 3(d) isolates the effect of total pressure, which is varied while keeping both the residence time and the inlet reactant partial pressures fixed. We find that the primary cause for the effect of total pressure on the H concentration is the effect of total pressure on diffusion, and the associated diffusive loss of H atoms to surfaces. As the pressure is increased from 0.6 to 1.5 Torr, radicals, including H, build up rapidly, and initiate chain-branching reactions. The increased concentration of

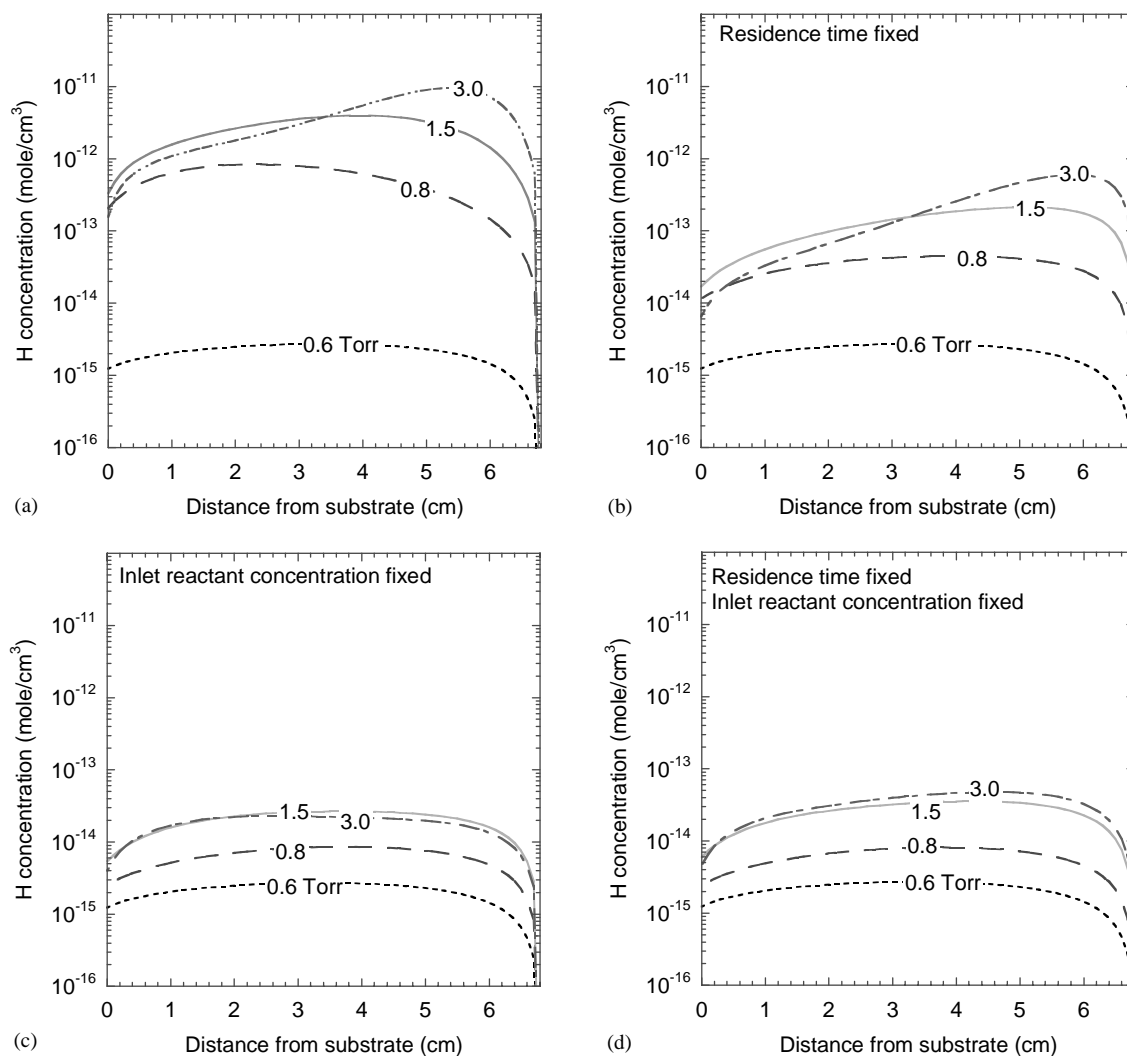


Fig. 3. The effect of system parameters associated with total pressure change on H concentration profiles at $T_s = 800^\circ\text{C}$, $R = 20$ and 200 sccm: (a) H concentration varying total pressure, (b) H concentration varying total pressure with residence time fixed, (c) H concentration varying total pressure with inlet reactant concentration fixed and (d) H concentration varying total pressure with both the residence time and inlet reactant concentration fixed.

radicals as the pressure increases from 0.6 to 1.5 Torr, even by the relatively modest factors seen in Fig. 3(d), results in an exponential increase in particle production, as shown below in Fig. 9. However, as the pressure is further increased above 1.5 Torr, the pressure sensitivity is lost. There are two reasons for this: (1) the radical diffusivity becomes smaller at higher pressures, and (2) the chemistry becomes precursor limited due to species depletion caused by particle nucleation and surface growth.

The change in temperature profiles with respect to pressure, shown in Fig. 2(d), may also play a role in the chemical kinetics of radicals. However, it is seen that the correlation between the H

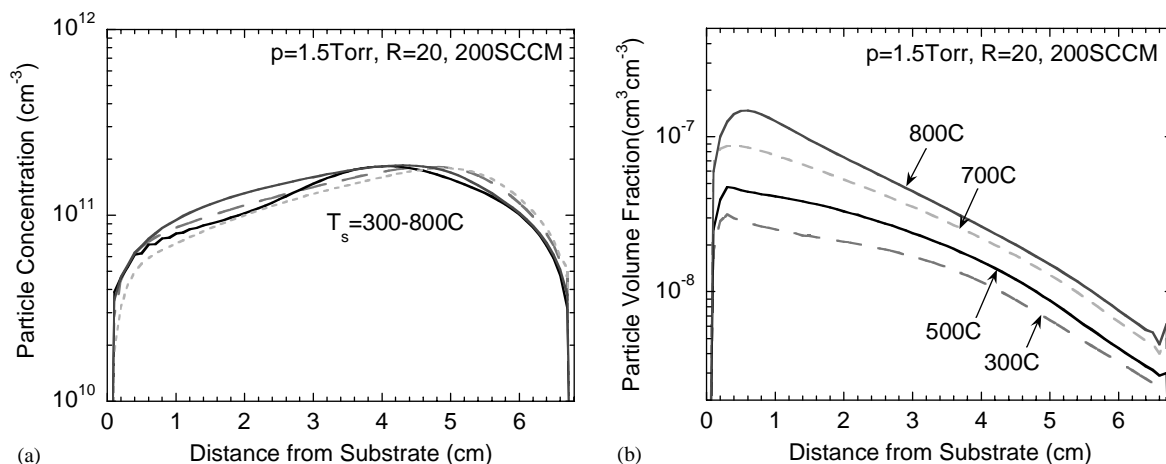


Fig. 4. Substrate temperature effect on particle concentration and size at 1.5 Torr, $R = 20$ and 200 sccm: (a) axial distributions of particle concentration and (b) axial distributions of particle volume fraction.

concentration profiles in Fig. 3(a) and the temperature profiles in Fig. 2(d) is not strong, particularly in that the large temperature increase for a pressure change from 0.8 to 3.0 Torr does not affect the H concentration as much as does the pressure change from 0.6 to 0.8 Torr. It is also worth noting that the predicted H concentration profiles shown in Fig. 3 depend on its surface reactivity—a unity sticking probability was assigned for all radicals in this study—which can affect the significance of the role of radicals in the results.

Fig. 4 shows the effect of substrate temperature on particle concentration and volume fraction. The pressure is set at 1.5 Torr with a flow of 200 sccm and oxygen-to-silane ratio of $R = 20$, while T_s varies from 300°C to 800°C. Fig. 4(a) clearly indicates that substrate temperature has little or no influence on particle number concentration. This is not a surprising result, as unlike the case of silane pyrolysis, which requires thermal activation, the chemistry of silane oxidation does not. Rather, as explained above, the chemistry is driven by highly reactive radicals which play a key role in chain-branching reactions, and thus in the destruction of silane. These chain-branching reactions are essentially barrierless processes and occur at a much faster rate than thermal decomposition of silane.

In contrast to the particle concentrations' insensitivity to T_s , particle volume fraction, shown in Fig. 4(b), is predicted to increase by up to an order of magnitude as the substrate temperature changes from 300°C to 800°C. At higher temperatures increased surface reaction rates increase the particle surface growth rate, which results in larger particles and thus higher particle volume fractions. Fig. 4(b) also shows that the maximum values of particle volume fraction are shifted slightly closer to the substrate at lower substrate temperatures. As with the effect of pressure (discussed above in connection with Fig. 2(c)), varying the substrate temperature affects the location of the point where thermophoretic and convective forces are balanced, allowing particles maximum time to grow. The local peaks near the showerhead can similarly be explained by a local balance of thermophoretic and convective forces.

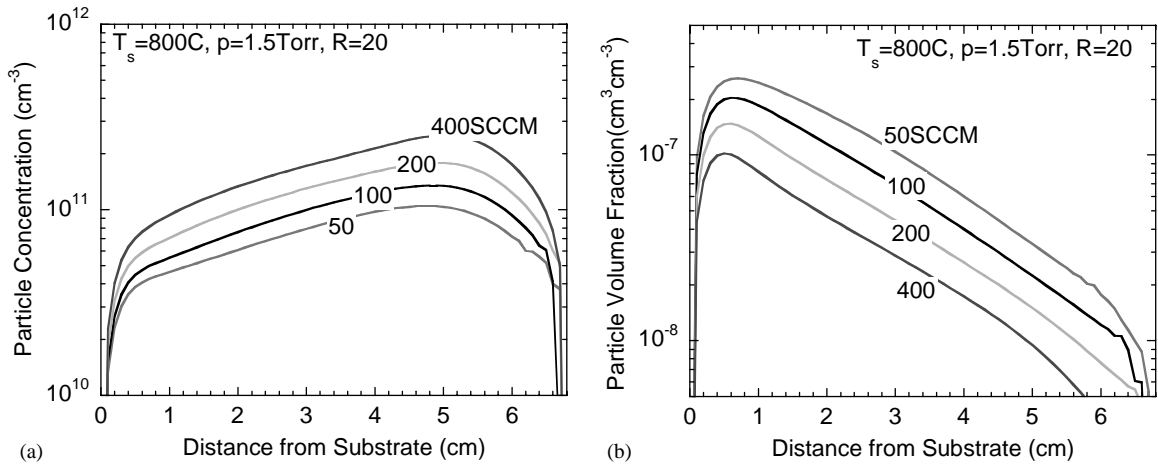


Fig. 5. Inlet mass flow rate effect on particle concentration and size at 1.5 Torr, $R = 20$ and $T_s = 800^\circ\text{C}$: (a) axial distributions of particle concentration and (b) axial distributions of particle volume fraction.

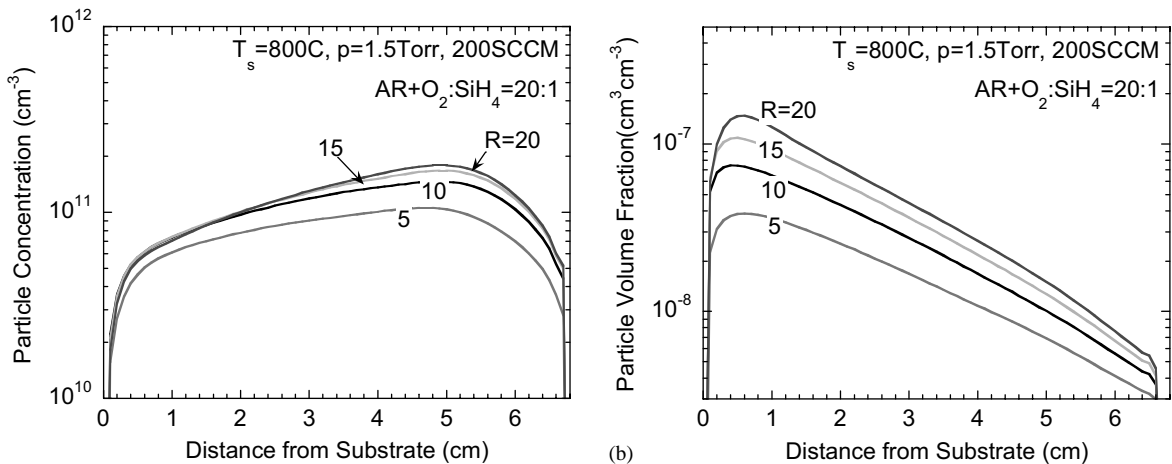


Fig. 6. Effect of oxygen-to-silane ratio (R) on particle concentration and size at 1.5 Torr, $T_s = 800^\circ\text{C}$ and 200 sccm: (a) axial distributions of particle concentration and (b) axial distributions of particle volume fraction.

The effect of flow rate is shown in Fig. 5, for a reactor pressure of 1.5 Torr, $T_s = 800^\circ\text{C}$ and $R = 20$. These results are mainly due to a residence time effect. At lower flow rates, particles have more time to grow either by coagulation or by surface reactions, thus Fig. 5(a) and (b) predicts lower particle concentration and higher volume fraction as the flow rate decreases.

We investigate the effect of the oxygen-to-silane ratio in Fig. 6 by varying the partial pressure of oxygen. Both the total pressure and the partial pressure of silane are kept constant by adjusting the partial pressure of an inert bath gas, argon. Both the particle concentration and the volume fraction are shown to increase with R in Fig. 6(a) and (b). Assuming the stoichiometry of the overall silane oxidation chemistry to be $\text{SiH}_4 + 2\text{O}_2 \rightarrow \text{SiO}_2 + 2\text{H}_2\text{O}$ (Hartman, Famil-Ghiriha, Ring, & Neal,

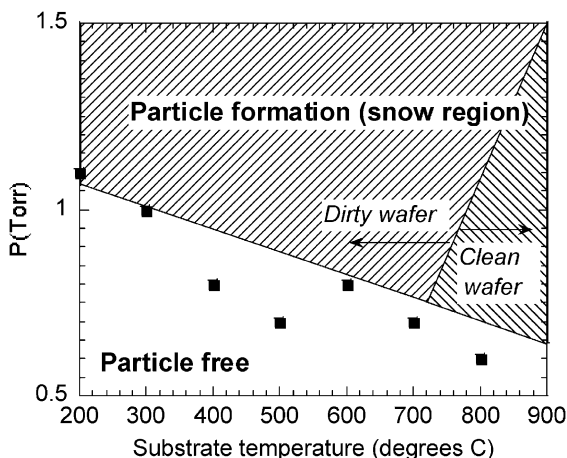


Fig. 7. Pressure-temperature diagram of particle formation regime. Filled squares represent experimental data at 200 sccm and $R = 20$ (by courtesy of T. Kim and P. McMurry (Kim et al., 2002)).

1987), excess oxygen at a condition with $R > 2$ might have been considered chemically unimportant. In fact, excess oxygen has a role in producing important chain carriers, H, OH and O, which can affect the silane decomposition process. Our calculations showed that, for an increase of R from 5 to 20, the silane decomposition rate increased from 35% to 58%, resulting in an increase in particle concentration and volume fraction by about a factor of two and four, respectively.

Fig. 7 compares the experimentally observed results for significant particle production (Kim, Suh, Girshick, Zachariah, McMurry, Rassel, Shen, & Campbell, 2002) with the model predictions at various substrate temperatures. The experiments were conducted in a reactor with the same geometry as in the model at 200 sccm and $R = 20$. The experimental data points represent the minimum pressure at which particles were detected for a given substrate temperature, and are shown to be in reasonably good agreement with model predictions (solid lines). The predicted boundaries of particle free and particle formation regimes are determined by the sensitivity of particle nucleation rate (J) to pressure (p) change: $d \log J / d p \geq 10$ when $J \geq 10^{12} \text{ cm}^{-3} \text{ s}^{-1}$. It is seen that there is only a small dependence of particle production on substrate temperature, in that particle production tends to be initiated at a lower pressure as the substrate temperature increases. It is also interesting to note that the model predicts two distinct regimes, a clean wafer regime and a dirty wafer regime, even during the formation of particles in the gas phase. The two regimes are determined by the direction of the calculated mass flux of particles due to convection and thermophoresis near the substrate. The clean wafer regime corresponds to particle mass flux directed upward from the substrate as a result of the large repulsive thermophoretic force at high substrate temperatures. Obviously a diffusive flux of particles to the substrate exists and may not be negligible especially for particles smaller than a few nanometers, but its contribution is not accounted for in defining the clean wafer regime for simplicity. As the pressure increases, the effect of the substrate-temperature-induced thermophoretic force becomes counterbalanced and is finally dominated by the exothermicity of the gas-phase chemistry, which reduces the temperature gradient near the substrate by heating the gas, and by the increased particle production due to the reactant partial pressure increase.

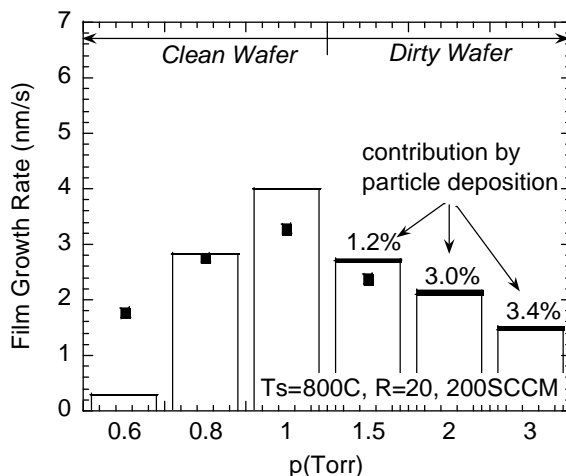


Fig. 8. Film growth rate at $T_s = 800^\circ\text{C}$, $R = 20$ and 200 sccm for various pressures. Filled squares represent experimental data (by courtesy of R. Russel and S. Campbell (Kim et al., 2002)).

Fig. 8 shows the predicted film growth rate for the same system parameters as in Fig. 7. Filled squares indicate experimental data (Kim et al., 2002). This figure together with Fig. 7 may provide a process design guideline by which an optimum operating condition can be found that seeks to maximize film growth rate, while still avoiding particle contamination. Film growth rate is shown to increase with pressure over the lower part of the pressure range because silane decomposition increases with total pressure. However, at pressures higher than 1.0 Torr, gas species depletion resulting from particle production becomes significant, and accordingly the film growth rate decreases with pressure. Moreover at the higher pressures, particle deposition to the film is shown to increase, as the higher gas temperature reduces the thermophoretic shielding effect. It should be pointed out that the model predictions of film growth rates together with particle diameters are highly dependent on the assumed surface reactivities of the gas species, which in general have considerable uncertainty. The currently assumed values of sticking probabilities produced reasonable agreement with experimental data on film growth rates (Kim et al., 2002), as seen in Fig. 8. However, recognizing that the results might be particularly sensitive to the sticking probability assumed for SiO, which has considerable uncertainty, we also ran simulations in which the SiO sticking probability was varied from the currently assumed 10^{-4} to 10^{-2} and 1. The result was that the particle surface growth rate increased by 10% and 54%, respectively, producing an increase in the peak median diameter by factors of 2 and 8, respectively. While not conclusive in itself, this result lends support to the conclusion of Buss et al. (1993) that the SiO molecule has low reactivity on silicon oxide films.

Inlet reactant concentrations are fixed in Fig. 9 to single out the effect of total pressure on film growth and particle production. Silane and oxygen concentrations are kept constant at, respectively, 2.6×10^{14} and $5.2 \times 10^{15} \text{ cm}^{-3}$ throughout the pressure change. The concentration of an inert bath gas, argon, is varied to change the total pressure. The other parameters are kept the same as in Fig. 8. Fig. 9(a) shows that film growth rates do increase with increasing total pressure for the lower pressure range, although the predicted values are lower than the rates in Fig. 8 in which the inlet reactant partial pressures scale with total pressure. The change of film growth rates with

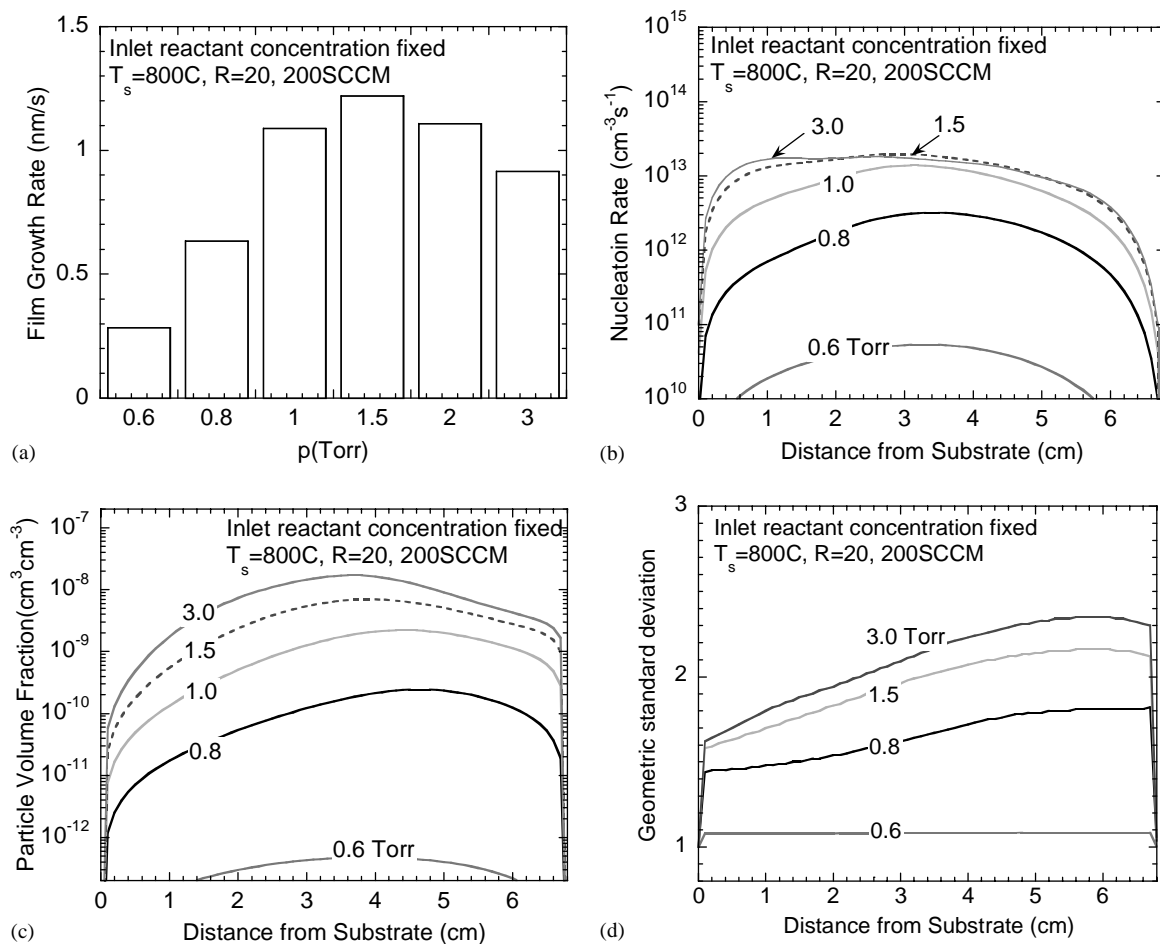


Fig. 9. Effect of total pressure on particle production at a fixed silane concentration of $2.6 \times 10^{14} \text{ cm}^{-3}$. $T_s = 800^\circ\text{C}$, 200 sccm and $R = 20$ with argon as bath gas: (a) predicted film growth rates, (b) axial distributions of particle nucleation rate, (c) axial distributions of particle volume fraction and (d) axial distributions of geometric standard deviations.

total pressure at pressures below 1.5 Torr can be attributed to the decomposition of silane, which increases from 1.3% to 27% for a pressure change from 0.6 to 1.5 Torr. At the same time, the particle nucleation rate is also predicted to change dramatically with pressure (for the lower pressure cases) as shown in Fig. 9(b), similar to Fig. 2(a). As pointed out with regard to Figs. 2 and 3, loss of radicals to the walls at the low pressures results in a sharp decrease in silane decomposition despite the fact that the inlet silane concentration is held constant. This decrease in silane decomposition translates into a decrease in film growth rate as well. As the pressure is increased above 1.0 Torr, however, the rate of increase of film growth is reduced, and finally the film growth rate decreases with increasing pressure above 1.5 Torr due to gas species depletion resulting from particle nucleation and subsequent growth, as implied in Fig. 9(c) by the steady increase in particle volume fraction with pressure. As shown in Fig. 9(d), the geometric standard deviation of the particle size distribution, which is assumed to remain lognormal, increases with pressure, as the

increased rates of both particle nucleation and coagulation at higher pressures result in a broader size distribution.

4. Summary

A model was developed to investigate particle formation during low-pressure chemical vapor deposition of silicon dioxide films from silane and oxygen. A detailed kinetics model for silicon oxide clustering was coupled to a moment-type aerosol dynamics model in an axisymmetric stagnation-point flow reactor. The nucleation rate, obtained from the clustering mechanism, was used as a source term in a moment-type aerosol dynamics model, where a lognormal particle size distribution function was assumed. We considered particle growth by surface reactions and coagulation, and particle transport by convection, diffusion and thermophoresis. Simulations were conducted to predict steady-state spatial distributions of major particle characteristics such as particle concentration, diameter, and volume fraction. The effects of various system operating parameters were assessed.

It was shown that pressure has the most dramatic effect on particle formation, especially at pressures below 1 Torr. Our results suggest design guidelines for achieving maximum film growth rates while minimizing particle contamination on the deposition surface.

Acknowledgements

This work was partially supported by the National Science Foundation (grant CTS-9909563) and by the University of Minnesota Supercomputing Institute.

References

- Babushok, V. I., Tsang, W., Burgess Jr., D. R., & Zachariah, M. R. (1998). Numerical study of low- and high-temperature silane combustion. *Twenty-seventh Symposium (International) on Combustion*, University of Colorado, Boulder, The Combustion Institute 2431–2439.
- Buss, R. J., Ho, P., & Weber, M. E. (1993). Laser studies of the reactivity of SiO with the surface of a depositing film. *Plasma Chemistry and Plasma Processing*, 13, 61–76.
- Coltrin, M. E., Kee, R. J., & Evans, G. H. (1989). Mathematical model of the fluid mechanics and gas-phase chemistry in a rotating disk chemical vapor deposition reactor. *Journal of the Electrochemical Society*, 136, 819–829.
- Coltrin, M. E., Kee, R. J., Evans, G. H., Meeks, E., Rupley, F. M., & Grcar, J. F. (1991). *SPIN: A program for modeling one-dimensional rotating disk/stagnation-flow chemical vapor deposition reactors*. SAND91-8003, Sandia National Laboratories, Albuquerque, NM.
- Dean, A. M. (1985). Predictions of pressure and temperature effects upon radical addition and recombination reactions. *Journal of Physical Chemistry*, 89, 4600–4608.
- Frenklach, M., & Warnatz, J. (1987). Detailed modeling of PAH profiles in a sooting low-pressure acetylene flame. *Combustion Science and Technology*, 51, 265–283.
- Friedlander, S. K. (2000). *Smoke, dust and haze: Fundamentals of aerosol behavior*. New York: Wiley.
- Girshick, S. L., Swihart, M. T., Suh, S.-M., Mahajan, M. R., & Nijhawan, S. (2000). Numerical modeling of gas-phase nucleation and particle growth during chemical vapor deposition of silicon. *Journal of the Electrochemical Society*, 147 (6), 2303–2311.
- Grcar, J. F. (1996). *The twopoint program for boundary value problems*. SAND91-8230, Sandia National Laboratories, Albuquerque, NM.

- Hargis Jr., P. J., Greenberg, K. E., Miller, P. A., Gerardo, J. B., Torczynski, J. R., Riley, M. E., Hebner, G. A., Roberts, J. R., Olthoff, J. K., Whetstone, J. R., Van Brunt, R. J., Sobolewski, M. A., Anderson, H. M., Splichal, M. P., Mock, J. L., Bletzing, P., Garscadden, A., Gottscho, R. A., Selwyn, G., Dalvie, M., Heidenreich, J. E., Butterbaugh, J. W., Brake, M. L., Passow, M. L., Pender, J., Lujan, A., Elta, M. E., Graves, D. B., Sawin, H. H., Kushner, M. J., Verdeyen, J. T., Horwath, R., & Turner, T. R. (1994). The gaseous electronics conference radio-frequency reference cell: A defined parallel-plate radio-frequency system for experimental and theoretical studies of plasma-processing discharges. *Review of Scientific Instruments*, 65, 140–154.
- Hartman, J. R., Famil-Ghirriha, J., Ring, M. A., & O'Neal, H. E. (1987). Stoichiometry and possible mechanism of SiH₄-O₂ explosions. *Combustion and Flame*, 68, 43–56.
- Kee, R. J., Rupley, F. M., Meeks, E., & Miller, J. A. (1996). *CHEMKIN III: A Fortran Chemical Kinetics Package for the analysis of gas-phase chemical and plasma kinetics*. SAND96-8216, Sandia National Laboratories, Albuquerque, NM.
- Kim, T., Suh, S.-M., Girshick, S. L., Zachariah, M. R., McMurry, P. H., Rassel, R. M., Shen, Z., & Campbell, S. A. (2002). Particle formation during low-pressure chemical vapor deposition from silane and oxygen; measurement, modeling and film properties. *Journal of Vacuum Science and Technology A*, 20, 413–423.
- Lee, K. W., Chen, H., & Gieseke, J. A. (1984). Log-normally preserving size distribution for Brownian coagulation in the free-molecule regime. *Aerosol Science and Technology*, 3, 53–62.
- Liehr, M., & Cohen, S. A. (1992). Low pressure chemical vapor deposition of oxide from SiH₄/O₂: Chemistry and effects on electrical properties. *Applied Physics Letters*, 60, 198–200.
- McQuarrie, D. A. (1976). *Statistical mechanics*. New York: Harper & Row.
- Meeks, E., Larson, R. S., Ho, P., Apblett, C., Han, S. M., Edelberg, E., & Aydil, E. S. (1998). Modeling of SiO₂ deposition in high density plasma reactors and comparisons of model predictions with experimental measurements. *Journal of Vacuum Science and Technology A*, 16, 544–563.
- Nayak, S. K., Rao, B. K., Khanna, S. N., & Jena, P. (1998). Atomic and electronic structure of neutral and charged Si_nO_m clusters. *Journal of Chemical Physics*, 109, 1245–1250.
- Pratsinis, S. E., & Kim, K.-S. (1989). Particle coagulation, diffusion, and thermophoresis in laminar flows. *Journal of Aerosol Science*, 20, 101–111.
- Schlichting, H. (1979). *Boundary-layer theory*. New York: McGraw-Hill.
- Semiconductor Industry Association, (1999). *International technology roadmap for semiconductors*. Austin, TX, USA.
- Smooke, M. D., McEnally, C. S., Pfefferle, L. D., Hall, R. J., & Colket, M. B. (1999). Computational and experimental study of soot formation in a coflow, laminar diffusion flame. *Combustion and Flame*, 117, 117–139.
- Suh, S.-M., Zachariah, M. R., & Girshick, S. L. (2001). Modeling particle formation during low-pressure silane oxidation: Detailed chemical kinetics and aerosol dynamics. *Journal of Vacuum Science and Technology A*, 19, 940–951.
- Swihart, M. T., & Girshick, S. L. (1999). Thermochemistry and kinetics of silicon hydride cluster formation during thermal decomposition of silane. *Journal of Physical Chemistry B*, 103, 64–76.
- Waldmann, L., & Schmidt, K. H. (1966). *Thermophoresis and diffusiophoresis of aerosol*. New York: Academic Press.
- Westmoreland, P. R., Howard, J. B., Longwell, J. P., & Dean, A. M. (1986). Prediction of rate constants for combustion and pyrolysis reactions by bimolecular QRRK. *A.I.Ch.E. Journal*, 32, 1971–1979.
- Zachariah, M. R., & Tsang, W. (1995). Theoretical calculation of thermochemistry, energetics, and kinetics of high-temperature Si_xH_yO_z reactions. *Journal of Physical Chemistry*, 99, 5308–5318.